Water Resources Research

RESEARCH ARTICLE
10.1029/2021WR031710

Special Section:
Advancing process representation in hydrologic models: Integrating new concepts, knowledge, and data

Stochastic Modeling Approach to Identify Uncertainties of Karst Conduit Networks in Carbonate Aquifers

S. Banusch[1], M. Somogyvári[1], M. Sauter[2], P. Renard[3,4], and I. Engelhardt[1]

[1]Department of Hydrogeology, Technische Universität Berlin, Berlin, Germany, [2]Department of Applied Geology, Georg-August-University Göttingen, Berlin, Germany, [3]Centre for Hydrogeology and Geothermics, Université de Neuchâtel, Neuch, Switzerland, [4]Department of Geosciences, University of Oslo, Berlin, Norway

Key Points:

- We statistically generate multiple sets of karst conduit network geometries using input data based on soft information
- The resulting Karst Probability Map accounts for uncertainty in the spatial distribution of the karst conduit network
- Our approach can assist in the integration of soft information into the parametrization of karst groundwater models

Correspondence to:
I. Engelhardt,
irina.engelhardt@tu-berlin.de

Citation:
Banusch, S., Somogyvári, M., Sauter, M., Renard, P., & Engelhardt, I. (2022). Stochastic modeling approach to identify uncertainties of karst conduit networks in carbonate aquifers. *Water Resources Research*, *58*, e2021WR031710. https://doi.org/10.1029/2021WR031710

Received 29 NOV 2021
Accepted 13 JUL 2022

Author Contributions:
Conceptualization: I. Engelhardt
Funding acquisition: I. Engelhardt
Investigation: I. Engelhardt
Methodology: I. Engelhardt
Project Administration: I. Engelhardt
Resources: I. Engelhardt
Supervision: I. Engelhardt
Writing – original draft: I. Engelhardt
Writing – review & editing: I. Engelhardt

Abstract The characterization of the karst conduit network is an essential task to understand the complex flow system within karst aquifers. However, this task is challenging and often associated with uncertainty. Equivalent porous media approaches for modeling flow in karst aquifers fall short of capturing the hydraulic effect of individual karst features, while process-oriented karst evolution models imply major computational efforts. In this study, we apply the Stochastic Karst Simulator (SKS) developed by Borghi et al. (2012) to generate karst conduit networks at a regional scale of a highly karstified carbonate aquifer located in the Eastern Mediterranean region and extensively used for water supply. The SKS generates conduit network geometries reasonably quick, using a mathematical proxy that mimics conduit evolution. The conduit simulation is based on a conceptual model of the genesis of the aquifer, consisting of different karstification phases. The stochastic approach of the algorithm enables us to generate an ensemble of conduit network realizations and to represent the uncertainties of these simulations in a Karst Probability Map. With only soft input information to constrain conduit evolution, multiple equivalent realizations yield similar resulting network geometries, indicating a robust approach. The presented methodology is numerically efficient, and its input can be easily adjusted. Subsequently, the resulting stochastic spatial distribution of conductivities can be employed for the parametrization of regional karst groundwater models.

1. Introduction

Karst aquifers exist in all climate zones and constitute crucial water resources. Analyses by Goldscheider et al. (2020) showed that approximately 15% of the global ice-free land surface consists of carbonate rock, and Stevanović (2019) estimated that around 9% of the world population consumes water from karst resources. Karst aquifers are characterized by highly permeable conduits embedded in a less permeable porous rock matrix. Most of the groundwater flow in karst aquifers is therefore controlled by the conduits, which form complex, hierarchically organized networks (Ford & Williams, 2007). Thus, the conduit network dominates the hydraulic properties of karst aquifers. To adequately represent these flow dynamics, it is vital to account for the spatial distribution of the conduits. However, this task is often associated with challenges and uncertainties due to the large scale and complexity of karst aquifer systems (Bakalowicz, 2005).

Numerical groundwater models are essential tools for addressing groundwater-related problems, for example, water resources assessment, and have been widely applied to study karst aquifers (Anderson et al., 2015; Parise et al., 2018; Zanini et al., 2021). Global model approaches, that link recharge estimations to spring discharge time series, provide information on the hydraulic behavior of the entire karst system, but do not provide detailed information on the hydraulic parameter field and therefore lack predictive power for climatic and geo-hydraulic interactions (Eisenlohr et al., 1997; Kovács & Sauter, 2007). Advanced model approaches for conduit networks are based on the speleogenetic evolution of karst aquifers (Kaufmann et al., 2019; Liedl et al., 2003). These models solve complex coupled process equations of chemical carbonate dissolution and groundwater flow with major computational effort (Bauer et al., 2003). Incorporating stochastic approaches into the modeling process provides the opportunity to evaluate uncertainties related to the resulting spatial distribution and geometry of a conduit network. A stochastic model approach developed by Jaquet et al. (2004) focuses on integrating conservative and reactive transport processes that control the conduit evolution such as advection, dispersion, and dissolution, but does not account for actual field observations of the karst system investigated. Further approaches by Frantz et al. (2021) and Pardo-Igúzquiza et al. (2012) simulate the conduit's geometry stochastically, based on field data of the dimensions of known conduit segments. However, these data are normally laborious to obtain,

Figure 1. (a) Overview map of the model area located within the Western Mountain Aquifer (WMA) indicating the two major springs and recharge area of the karst system. (b) Regional overview and outline of the whole karst aquifer.

and the information is highly downscaled and difficult to be generalized to large-scale catchment-based analyses.

The conduit network in this study is generated by the "Stochastic Karst Simulator" (SKS; Borghi et al., 2012). The SKS algorithm uses only limited input information that is, input that controls conduit evolution, such as the spatial distribution of regional hydrogeological units, structural heterogeneities (faults and fractures), and the positions of inlet and outlet locations as well as ancient (paleo) recharge and base level conditions. Numerical approximation of the underlying physics, without solving complex flow equations and accounting for dissolution processes, makes the SKS algorithm numerically efficient. This, in turn, enables the generation of multiple equivalent realizations of conduit networks and allows for stochastic analysis. Previous studies applied the SKS algorithm to small-scale karst aquifer systems, investigating only one phase of karst development. Therefore, limited input data variation was implemented and the uncertainty in conduit network geometry was only partially investigated (Borghi et al., 2016; Fandel et al., 2021; Sivelle et al., 2020; Vuilleumier et al., 2013).

This study applies the SKS algorithm to generate karst conduit networks at a regional scale of a highly karstified carbonate aquifer located in the Eastern Mediterranean region. We focus on integrating different phases of karstification of the aquifer system, which highly influences the connectivity of the subsequent conduit network. A stochastic analysis allows displaying the uncertainties embedded in the resulting conduit network reconstruction as a Karst Probability Map. This enables us to identify the most probable spatial distribution of the conduit network of the investigated aquifer system, which then serves as a basis for the parametrization of discrete numerical groundwater flow models.

To apply the algorithm on a regional scale, we develop a methodology that integrates all critical information to constrain the model, while at the same time reconstructing the conduit network reasonably for modeling purposes. Therefore, the aquifer system selected for the investigation should meet the following criteria: (a) being relevant for regional groundwater management, as crucial issues for sustainable management of these systems are often addressed by groundwater models. Furthermore, (b) a well-investigated aquifer by field observations such as borehole measurements is ideal. This is rare in karst aquifers, even if used for the local water supply since karst systems are usually tapped by the spring discharge only and less often by many pumping wells. Measurements in these boreholes can provide crucial insight for the verification of the approach before setting up a groundwater model with the parametrization given by the SKS algorithm. Applying the presented approach is also facilitated if (c) well-documented references of the karst genesis of the investigated aquifer system are available, to integrate different phases of karst development. Lastly, for the study to have (d) a large-scale aquifer system available, to go beyond previous applications of the SKS algorithm, where the algorithm has proven to be suitable to identify individual conduits in small karst catchments (<100 km^2). The karst system should finally (e) be geologically and structurally "simple" so that we can check the presented methodology without having to allow for special features in the aquifer system complicating matters. This criterion implies a manageable number of inlets, outlets, hydro-stratigraphic layers, and phases of karst development.

2. Materials and Methods

2.1. Study Site

In this study, we investigate the Western Mountain Aquifer (WMA), located in the Eastern Mediterranean region (Figure 1). It is a transboundary carbonate aquifer, underlying great parts of Israel and the West Bank

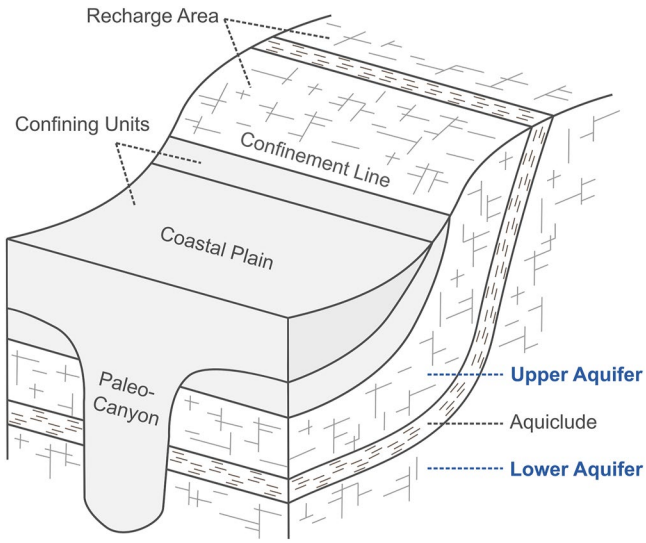

Figure 2. Schematic outline of the geological setting in the model area (illustration adapted after Laskow et al., 2011; UN-ESCWA & BGR, 2013; Weinberger et al., 1994). The Western Mountain Aquifer consists of two carbonate layers (Upper and Lower Aquifer), separated by a marl aquiclude layer. The karst aquifer system is confined below the coastal plain (with locally incised paleo-canyons) and changes to unconfined conditions in the central mountain range where it is recharged by infiltrating precipitation.

and providing crucial freshwater resources for both regions (Guttman, 2021; UN-ESCWA & BGR, 2013). The WMA consists of mainly limestone and dolomite formations of the Mid-Cretaceous Judea Group (JG; Bartov et al., 1981; Weinberger et al., 1994). The JG is generally divided into two carbonate aquifer horizons: Upper and Lower Aquifer separated by impermeable marl formations (Figure 2; Weinberger et al., 1994). The karst aquifer system reaches a maximum thickness of up to 800 m in the northern part and about 500 m in the south (Guttman, 2021). The WMA is confined in the coastal plain and changes to unconfined conditions in the central mountain range where the aquifer is exposed due to its anticlinal structure and the erosion of the overlying rocks (Figure 2). This area is considered the recharge area of the aquifer. Dafny et al. (2010) characterize the WMA as a mature karst aquifer, based on numerous direct and indirect observations such as pumping tests, cave investigations, and geophysical borehole measurements. Frumkin and Fischhendler (2005) describe today's landform in the recharge area as fluvio-karst, with overall well-developed surface drainage.

Precipitation infiltrating in the mountain range where the WMA is exposed is the main source of groundwater recharge (Figures 1a and 2) (Dafny et al., 2010; Guttman, 2021; Weinberger et al., 1994), with a mean annual precipitation of 490 mm. The climate is characterized by hot, dry summer periods and mild, rainy winters with an average annual temperature of 22°C. Groundwater recharge estimations from previous studies of the WMA suggest a close relationship between annual precipitation patterns and annual recharge, and range between 160 and 220 mm per year (Abusaada & Sauter, 2013; Dafny et al., 2010; Dvory et al., 2016; Sheffer et al., 2011). Groundwater flow is oriented from the recharge area toward the coastal plain and the aquifer discharges at the Yarkon and Taninim springs located in the central and northern part of the karst aquifer system (Figure 1a). After extensive exploitation of groundwater resources since the 1950s, natural discharge at both springs has been greatly reduced (Guttman, 2021).

This research investigates an area of approximately 6,000 km^2 located within the WMA (Figure 1a). The model area corresponds to the outline of the aquifer as described in Weinberger et al. (1994) (Figure 1b), but excludes the area south of Beersheba because groundwater resources beyond that area are known to contribute only little to the total groundwater flow of the karst system. The southern boundary of the model area in this study follows the Afiq canyon, a buried paleo-canyon filled with impermeable sediments, which runs through the complete karst aquifer system (Druckman et al., 1995). The Afiq canyon is part of a system of submarine canyons developed during the Oligocene. During the Late Miocene, a sharp sea-level drop in the Mediterranean basin, known as the Messinian Salinity Crisis and caused by tectonic processes that closed the Gibraltar straight (Garcia-Castellanos & Villaseñor, 2011; Krijgsman et al., 1999; Roveri et al., 2014), exposed the submarine canyons (Druckman et al., 1995). Today, these paleo-canyons are filled with Pliocene to Pleistocene sediments (Figure 2) and are deeply buried below the present-day coastline of Israel (Laskow et al., 2011).

2.2. Karst Conduit Network Generation

The karst conduit network for the WMA is simulated at a regional scale using the SKS developed by Borghi et al. (2012). The simulator focuses on modeling the main conduits in epigenetic karst systems, assuming that water follows a path of least resistance between inlet points (sinks, dolines) and outlets (springs) that is, the hydraulic gradient. The SKS approach consists of the following steps (Figure 3): (a) construction of a geological model, focused on the main hydro-stratigraphic units, (b) integration of information on hydraulically relevant structural elements, such as faults and fractures acting as initial pathways during the early phase of karstification, (c) identification of present-day recharge and discharge locations as well as those in the geological past, and lastly (d) simulation of the karst conduits. The SKS algorithm mimics conduit evolution during the simulation using a mathematical proxy, the Fast-Marching-Algorithm (FMA) by Sethian (1996, 1999, 2001). The FMA estimates for any given inlet location the shortest pathway to the outlet points, constrained by the structural

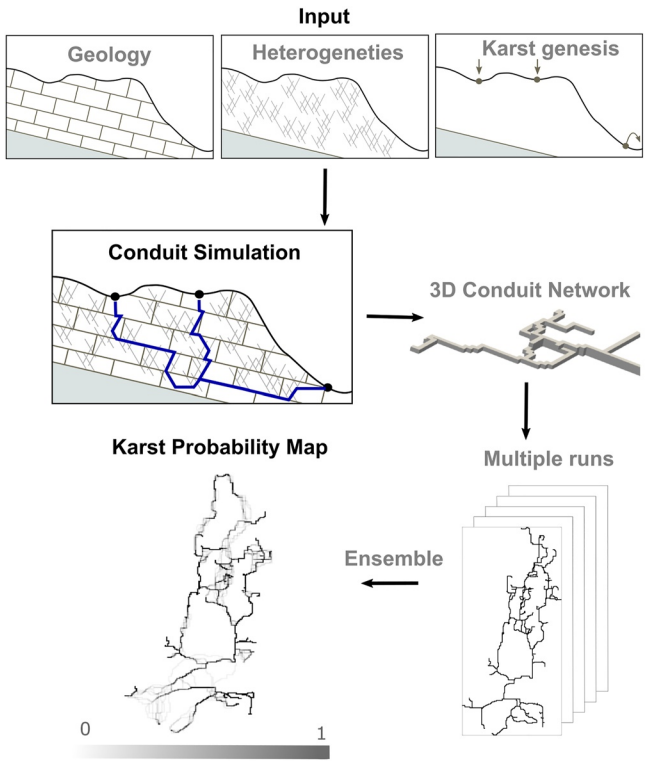

Figure 3. Overview of the presented approach to create a Karst Probability Map, consisting of 500 individual karst conduit network realizations. The conduits are simulated with the Stochastic Karst Simulator following Borghi et al. (2012). Input information consist of the geometry of the hydro-stratigraphic units, the position of structural elements such as faults and fractures, as well as inlet and outlet locations for recharge and discharge of the karst system derived from the geomorphological reconstruction of the karst aquifer genesis.

and hydrogeological input information. Particle tracking is then performed from the given inlets to the outlets. The resulting pathways are converted into karst conduits. Furthermore, the SKS computes hierarchical conduit networks based on multiple phases of karst development. With this approach, later phases of karst development can be superimposed on earlier ones that is, the hydraulic effect of pre-existing conduits influences the orientation and position of more recently developed pathways, as large initial conduits attract more water and are further widened by chemical dissolution. This approach is consistent with current conceptual knowledge of karst development (Bakalowicz, 2005; Bauer et al., 2003; Kaufmann & Braun, 2000).

2.3. Input Data for Conduit Simulation

Incorporating available information from reported field investigations is the main source of input to the SKS algorithm. Following that, the algorithm statistically accounts for features for which no field observations are available. This is even more challenging in the simulation of large-scale catchments for example, identifying the exact number and location of inlets and outlets to the karst system of which often only the most important that is, those with a prominent spring discharge are known.

The geological model of the WMA in this study is adapted from the model of Abusaada and Sauter (2013), which was constructed using MODFLOW-2000 (Hill et al., 2000). The model is grouped into four hydrogeological units based on the hydraulic conductivity of the formations (from bottom to top): Lower aquifer (carbonate formations), aquitard layer (low-permeability chalk and marl formations), Upper Aquifer (carbonate formations), and confinement layer (low-permeability; Figure 2). The extent of the geological model corresponds to the model area depicted in Figure 1. The grid cells are cubes with a grid spacing of 500 m. Each cell within the model domain is assigned to one of the four hydrogeological units. The applied geological model that is, its horizontal extent and the vertical extent of the carbonate layers strongly influence the position and properties of the simulated conduits because their relative extent is limited by these boundaries. Therefore, it is of vital importance to carefully consider the hydrogeological boundaries and study the geometry of the stratigraphic units.

Next, the structural properties of the aquifer layers are added. Faults and fractures act as initial pathways for the conduit development, later enlarged by chemical dissolution (Kaufmann & Braun, 2000). Input to the SKS is the digital structural map for the Judea Group by Fleischer and Gafsou (2003). Reverse faults in the map are associated with the Syrian Arc fold belt. Observations and analysis by Sagy et al. (2018) demonstrate a constant direction of Syrian-arc type folds trending NE-SW (28°–38°) throughout time regardless of ongoing tectonic processes in the surrounding areas. The SKS algorithm also provides a built-in Fracture Generator. It uses a stochastic approach for each fracture set, varying the following geometric fracture properties: density (probability of occurrence), length, and range of strike and dip information (Borghi et al., 2012). The Fracture Generator uses this information for the initial orientation of the first simulated conduits. However, the final orientation of the conduit network is different from the orientation of the fractures alone because the spatial distribution of the conduits is strongly influenced by the hydraulic gradient, determined by the position of discharge locations as well as the spatial distribution of recharge. Two main fracture sets are identified for the WMA after Eyal et al. (2001) and their derived parameters for the SKS algorithm are summarized in Table 1. The first fracture set is associated with the Dead Sea Transform (DS) and is generally oriented along an NNW-SSE axis. The second, which is dominant in the mountainous areas of the WMA area, is associated with the Syrian Arc Folding Event (SA) and is oriented in a WNW-ESE direction.

A conceptual karst genesis model of the WMA accounts for different paleo-hydrological conditions in the study area. Two phases of karst development are identified for the WMA with different discharge points to the karst

Table 1
Parameters Implemented in the Built-In Fracture Generator of the Stochastic Karst Simulator Algorithm (Borghi et al., 2012) for the Two Fracture Sets Identified for the WMA: Dead Sea Transform (DS) and Syrian Arc Folding Event (SA)

Parameter	Description	Value
NFrac	Total number of fractures to be generated for each karstifiable layer	1,000 (Upper Aquifer)
		1,500 (Lower Aquifer)
strikeMin	Minimum strike of the fracture families [°]	146 (DS), 88 (SA)
strikeMax	Maximum strike of the fracture families [°]	180 (DS), 125 (SA)
dipMin	Minimum dip of the fracture families [°]	79 (DS), 75 (SA)
dipMax	Maximum dip of the fracture families [°]	90 (DS), 90 (SA)
fractureLength	Length of the generated fractures [m]	111

system due to changing base level conditions in the region (Figure 4). Phase 1 occurred during the Messinian Salinity Crisis when the Mediterranean Sea levels dropped sharply. It is assumed, that during this period the submarine canyons were exposed and functioned as discharge points to the karst system (Druckman et al., 1995; Laskow et al., 2011). It is further assumed, that this has formed an E-W trending flow regime. The position of the canyons is defined after Laskow et al. (2011). Phase 2 indicates the modern-day natural outlets of the karst system: the Yarkon and Taninim spring, located 18 and 3 m above sea level, respectively. During this second phase, the flow regime is shifted toward an S-N trend in the confined part of the aquifer. The recharge area, and therefore the inlet points to the WMA karst system, can be assumed to be largely the same throughout the karst development (Frumkin & Fischhendler, 2005).

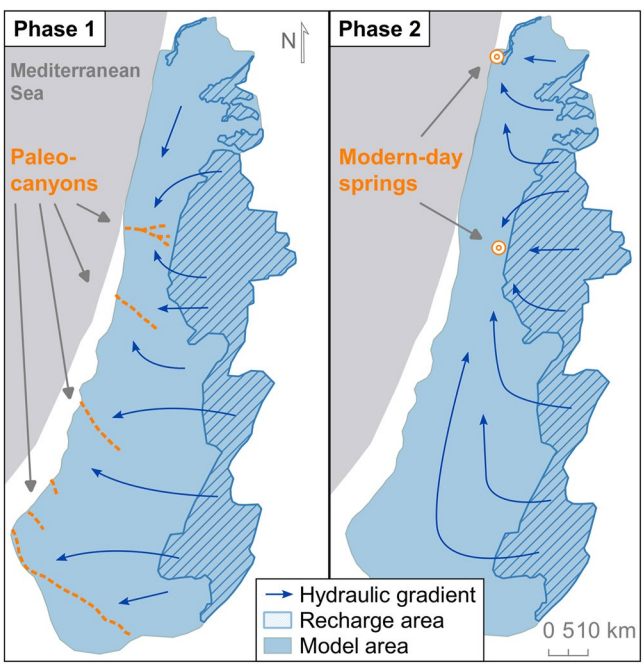

Figure 4. Conceptual model of the Western Mountain Aquifer karst genesis: two phases with different discharge locations of the karst system are identified. The paleo-canyons are outlined after Laskow et al. (2011).

2.4. Implementation

The SKS model is defined across the same domain as the geological model of the WMA. It is specified with a coarse resolution (500 m) to allow for a stochastic analysis by keeping computational times at a minimum, while still accounting for the hydrogeological setting of the investigated aquifer. The conduits are modeled to follow along the edges of the model grid cells as one-dimensional pipes (Borghi et al., 2012). The cells corresponding to the conduits are marked as conduit elements in the resulting network. The two aquifer layers of the JG are defined as karstifiable formations. Recharge to the WMA is understood to occur as diffuse recharge within the mountain range where the karst system is exposed (Figure 1). No field data of individual sinks or dolines are available. The simulations are run with randomly generated inlet locations within the recharge area. For each run, 100 points are set, based on the high-resolution model grid, and the results show that inlet points close to each other quickly connect to form individual conduits. Two sets of outlet locations are used for a single SKS run derived from the conceptual karst genesis model of the WMA (Figure 4). The locations of discharge points for phase 1 karstification are generated randomly along the given paleo-canyon lineaments. For this initial phase of karstification, 20 outlet points are set. This number is also based on experience with the high-resolution model and the connection of very close outlet points into single conduits in the SKS. The locations of discharge points for phase 2 karstification are placed at the coordinates of the Yarkon and Taninim springs (Figure 1). The set inlet points are constant for both phases in each run. The outlets of the karst system are simulated in the same order as the phases, defining the connectivity of the resulting conduits.

2.5. Karst Probability Map

The SKS is a stochastic algorithm, and the conduit modeling approach is partly randomized. This means that each conduit network generated by the SKS has a different geometry. To exploit the stochastic nature of the SKS, we performed 500 independent simulations for the WMA, resulting in an ensemble of 500 karst conduit network realizations. The following parameters are randomized for the individual model runs: inlet locations (across the recharge area), fracture properties (Table 1), outlet locations (along paleo-canyons), and order in which the conduits are generated. Thus, the resulting realizations of the conduit network geometry are subject to statistical variability but weighted equally since they are all generated using the same boundary conditions. To visualize the generated data set in a statistically meaningful way, a Karst Probability Map is prepared. Probability maps are widely used to visualize ensembles of spatial information, such as the results of stochastic facies modeling (Jiménez et al., 2016) or fracture network simulations (Somogyvári et al., 2017). The Karst Probability Map is generated by averaging all generated karst conduit geometries. The averaging is performed pixel-by-pixel over the 500 model realizations of the ensemble.

2.6. Clustering of Karst Geometries

To determine representative geometries within the ensemble of karst conduit network realizations, a multidimensional scaling (MDS) approach is employed (Caers et al., 2010). The MDS method visualizes the differences between the individual realizations by projecting their relative distance into a Euclidian plane. The relative distance between the realizations is calculated pairwise by taking the absolute difference between the conduit network geometries as rasters, pixel-by-pixel. This provides a distance matrix for all realizations, which can be projected as a point cloud using the MDS scaling. The MDS point cloud is then used to cluster the realizations of the ensemble and to identify groups of characteristic conduit network geometries.

3. Results

3.1. Statistical Analysis of Conduit Realizations

Five hundred realizations for the WMA conduit network are generated using the SKS algorithm, with a computation time of ca. 210 s for a single run on a computer equipped with 32 RAM. The statistical analysis of this conduit network ensemble is depicted as a Karst Probability Map at a resolution of 500 × 500 m in Figure 5a. The map shows high probabilities at pixel locations with many realizations displaying conduits. Low values show pixel locations with only a few conduits. The pixel values can be interpreted in terms of probabilities of the relative degree of karstification. Figure 5b shows the frequency distribution of the depicted probabilities, and Figure 5c shows the sensitivity of the Karst Probability Map to two different parameterizations of the location of start and end points of the generated karst conduit networks.

Two trends in the principal orientation of the conduit network for the WMA are well reproduced by multiple realizations: a high number of conduits extending east to west, and those extending south to north. The first dominant conduit network "bundle" connects the mountainous recharge area of the aquifer in the east with the identified paleo-canyons in the western coastal plain of Israel, a result of phase 1 karstification. The second prominent conduit network "bundle" connects the recharge area in the east with the two modern-day outlets of the karst system in the central and northern part of the model area, representing the identified latter phase of karst development. Many of the S-N trending pathways branch off along pre-existing E-W trending ones, because of the implementation of later phases of karstification building on earlier ones in the SKS algorithm. Due to the randomly given location of inlets within the recharge area (as recharge to the WMA is understood to occur as diffuse recharge) and outlets along lineaments vs. exact locations for the initial phase of karstification, the start and end points of most of the conduits are vague. The frequency distribution of the Karst Probabilities in Figure 5b shows a definite skewness to the "less probable conduits." Every conduit ever simulated by the SKS in one of the five hundred model runs which are the basis of the Karst Probability Map is depicted in one of the pixels in Figure 5a. Therefore, the "least probable conduits" are over-represented in their frequency. If this is disregarded, an otherwise symmetric distribution and a less pronounced second peak at the "highly probable conduits" can be observed. Especially around the outlets (springs) of the karst system do these high certainties for a high degree of karstification occur. Figure 5c shows the sensitivity of the Karst Probability Map to two different parametrizations of the locations of inlet and outlet points. These results were obtained by generating

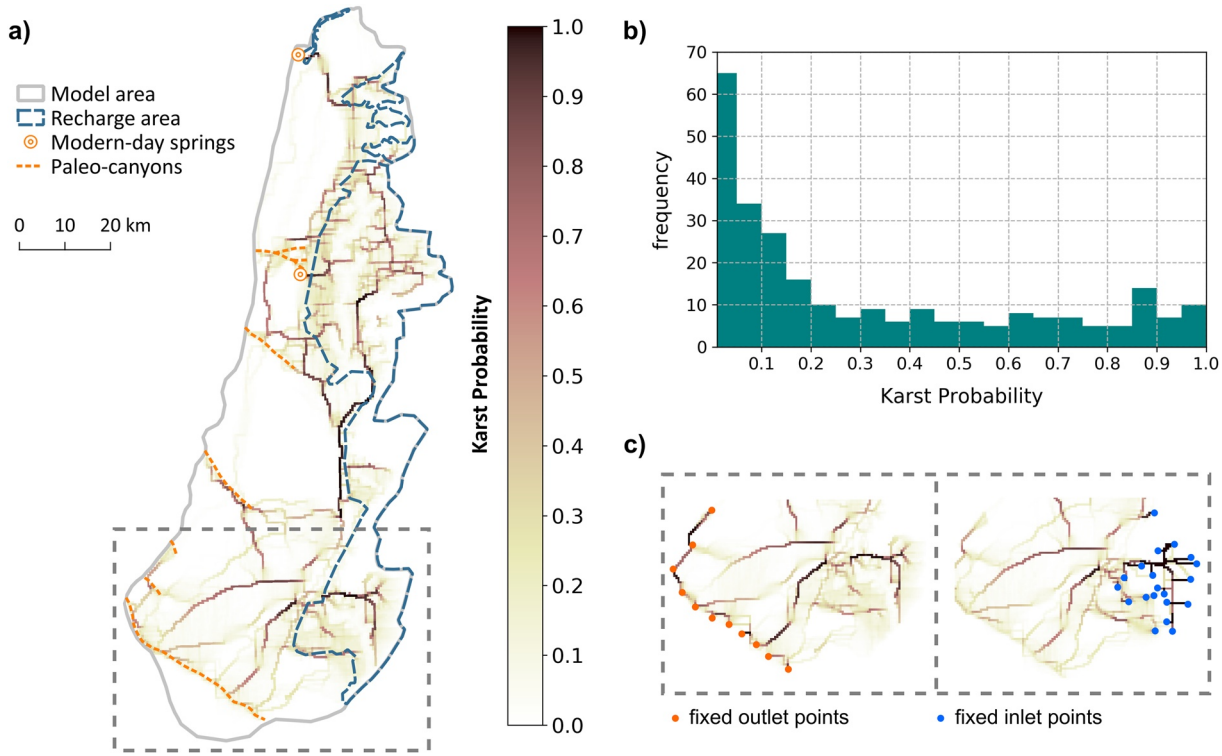

Figure 5. (a) Karst Probability Map of the Western Mountain Aquifer as an ensemble of 500 conduit network realizations, resolution 500 × 500 m. Pixel values are interpreted as the probability of a high degree of karstification. (b) Frequency distribution of the Karst Probabilities. (c) Sensitivity analysis of the given start and end points to the simulated karst networks in the southern part of the model domain.

500 realizations using the SKS algorithm, where we first positioned outlet points along the paleo-canyons to fixed locations and subsequently positioned the inlet points within the recharge area to fixed locations. The results of these simulations are shown in a zoom-in window for the southern part of the model domain. The fixed start and end points in each ensemble are indicated by orange and blue points (Figure 5c, respectively). The resulting Karst Probability Maps show that the changes in the spatial distribution of the probabilities are only marginal and localized around the inlets or outlets (compare Figure 5a with Figure 5c). The global patterns of the most probable locations of the conduits and the connectivity of the resulting conduit networks remain similar. These results demonstrate that the impact of the uncertain positions of inlet and outlet is low because their location only minimally affect the global geometry of the resulting conduit network. In addition, as the locations of in- and outlet points are not confirmed by field observations they are correctly represented by statistically varying their exact location within known boundaries.

3.2. Comparison of the Probability Map With Transmissivities and Previous Studies

Verifying the presented Probability Map for karst conduits is associated with some difficulties because of the complexity of such systems. Therefore, different approaches are conceivable depending on the availability of data on the investigated aquifer. The WMA is a highly exploited karst aquifer with numerous wells tapping its groundwater resources for domestic water supply and irrigation in a semi-arid climate. This has the advantage that borehole measurements during the installation of these pumping wells provide valuable insight into the structure of the WMA. Transmissivity data from 54 pumping wells in the model area is provided by Guttman (2021). Calculated from pumping test data, the resulting transmissivity values are understood as the integral of hydraulic conductivity integrated across the entire aquifer thickness. In this study, it is assumed that the magnitude of transmissivity corresponds to the degree of karstification in the area surrounding the pumping well for example, cone of depression. The Karst Probability Map is further compared to the Karst Abundance Map after Laskow et al. (2011), who present an approach to detect karst voids in the WMA by geophysical interpretations of borehole logs. In addition, we compare the Karst Probability Map to the given groundwater model discretization of

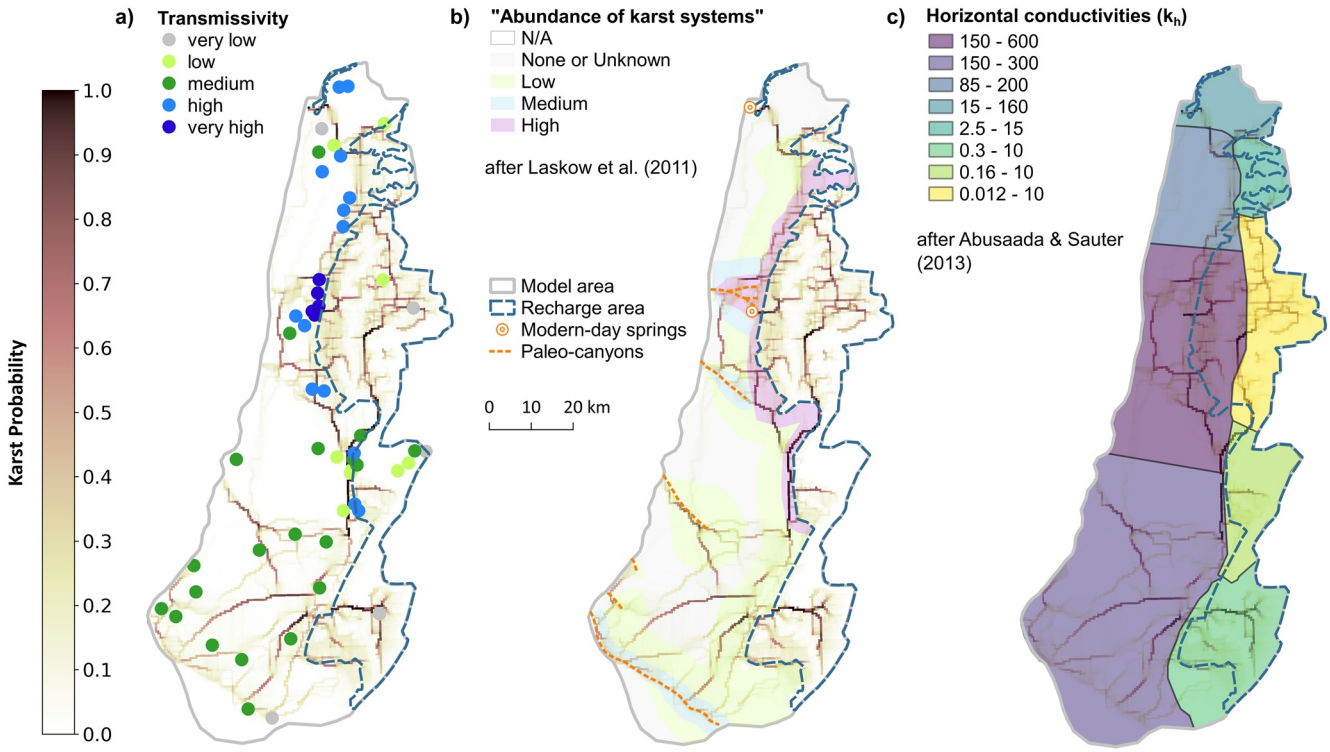

Figure 6. Comparison between the Karst Probability Map and (a) transmissivity measured in production wells in the model area ranging between very low ($<10^{-3}$), low (10^{-3}–10^{-2}), medium (10^{-2}–0.1) to high (0.1–1), and very high (>1) [m^2/s]; (b) "Karst Abundance Map" after Laskow et al. (2011). The unconfined part of the aquifer system (the recharge area) is not included in the study; (c) Model discretization of the horizontal conductivities (k_h) after Abusaada and Sauter (2013).

calibrated hydraulic conductivities of the WMA after Abusaada and Sauter (2013). The spatial distribution of the conduit network, together with the hydraulic properties of the limestone matrix determines the spatial distribution of the hydraulic conductivity field in karst aquifers. All comparisons are depicted in Figure 6.

Figure 6a shows the location of the pumping wells in the model area. The relative magnitude in transmissivity is divided into five categories ranging from very low ($<10^{-3}$ m^2/s) to very high (>1 m^2/s) and plotted over the presented Karst Probability Map. Figure 7 shows the distribution of transmissivity (T) of the 54 wells. Total values range between 1×10^{-4} and 1.7 m^2/s, with a mean transmissivity of 0.26 m^2/s, and most of the wells (37%) ranging between 1 to 8×10^{-2} m^2/s. At many locations in the model domain, there is a good agreement between the Karst Probability Map and measured transmissivities, especially since only "soft input information" is employed for the SKS modeling and the large size (ca. 6,000 km^2) of the model domain. The Karst Probability Map shows pronounced high degrees of karstification in three areas within the model domain: (a) in the area of the Yarkon spring in the central part of the model area, where higher intensities of karstification can be assumed because of flow convergence towards the spring, and (b) along the confinement line, which runs along the western border of the recharge area (Figures 1 and 2), explained by higher recharge rates at the boundary between less permeable marly and permeable limestone rocks, and (c) in the southern part of the model area, north of the city Beersheba. The highest transmissivities are also measured close to the Yarkon spring, and medium to high values along the northern and central confinement line. Medium transmissivity in the southern part of the model area is again in agreement with the simulated widespread karstification. The medium to high transmissivity area around the Taninim spring in the North is only partly

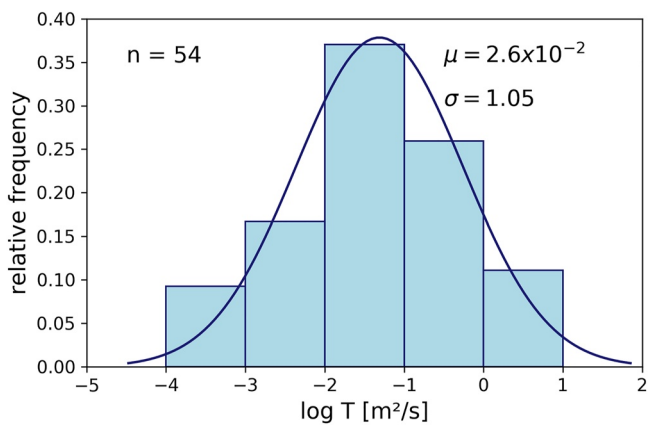

Figure 7. Histogram of transmissivity distribution in the model area, determined by pumping tests in groundwater abstraction wells. Data is provided by Mekorot Water Company Ltd.

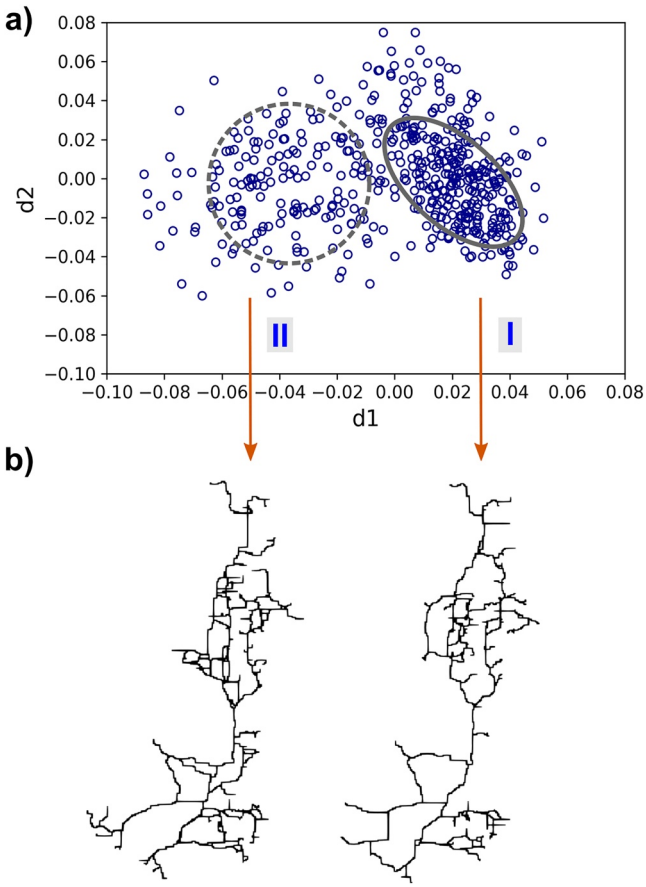

Figure 8. (a) Visualization of the 500 conduit network realizations using multidimensional scaling mapping with two identified clusters (I and II). (b) Representative karst conduit networks from clusters I and II.

depicted by the probability map. The same applies to the probability mapping within the recharge area, with diffuse recharge being assumed.

The "Abundance of karst systems" map after Laskow et al. (2011) in Figure 6b shows a high overlap with the presented Karst Probability Map. In both maps is the confinement line identified as an area of high permeability. Because both approaches account for different phases of karst development, is it possible to distinguish between overall low permeabilities in the coastal plain and increasing "karst abundance" closer to the paleo-canyons. As the unconfined part of the aquifer system (the recharge area) is not included in the study by Laskow et al. (2011), no comparisons can be drawn here. The biggest difference in the comparison of the two maps in Figure 6b can be seen in the southern part of the model domain, where there are several conduits indicated as highly probable by SKS connecting the southernmost Afiq paleo-canyon to the recharge area, whereas Laskow et al. (2011) only shows little to no karst abundance. The same applies to Taninim spring, the second outlet to the WMA, in the northernmost part of the aquifer. The degree of karstification in these areas requires further investigation that is, investigating how relevant these northernmost present-day and southernmost paleo-outlets are to the current flow dynamics of the WMA.

The model discretization of calibrated hydraulic conductivities by Abusaada and Sauter (2013) in Figure 6c is very coarse. The model domain is divided into eight discrete areas and within each category, there is a wide range of values. The interesting part though is to compare the model boundaries. There is a clear discretization between the southern, central, and northern model domains. This division is also well reproduced in the Karst Probability Map. The highest conductivities in both maps are depicting around the central Yarkon spring. The otherwise clear boundary between the poorly conductive recharge area and the highly conductive coastal plain within the model domain is not as clearly shown by the SKS. The comparison with an existing very coarse discretization of a groundwater model of the WMA shows how the Karst Probability Map can be applied to finer discretize existing groundwater models for the hydraulic parameters.

3.3. Representative Conduit Geometries

The Karst Probability Map indicates that the general geometry of the simulated conduit networks is similar to most realizations that is, the two trends in the principal orientation of the conduit network of the WMA are well reproduced. To identify possible representative karst conduit network geometries from within the ensemble, MDS is applied. The resulting point cloud is shown in Figure 8a. Note that the axes mean no absolute location but the relative difference between the plotted points that are representations of each model realization. These virtual dimensions are generated by the MDS projection which calculates a distance measure for each pairwise comparison of samples. The larger the distance, the lower the similarities. The resulting plot in Figure 8a shows good mixing, with one dominant and one less pronounced cluster. A representative conduit network from each of these two clusters is depicted in Figure 8b. The representative conduit network from cluster 1 shows a great resemblance with the high probability conduits in the karst map (colored dark red in Figure 5a). The less pronounced cluster 2 shows in general a more branched network geometry, with less straightforward conduits connecting points of recharge and discharge in the model domain. This indicates that cluster 1 represents those networks where the number of randomly generate inlet points (within the recharge area) and paleo-outlet points (along paleo-canyons) is close to each other, meaning they quickly converge to shared conduits and form less branched networks. This also explains the denser point cloud in Figure 8a and its resemblance to the high probability conduits in the Karst Probability Map, as this pattern seems to appear repeatedly. The less pronounced point cloud of cluster 2 demonstrates the wider range of resulting network geometries with a higher variability that is, larger grid spacing between the start and end points of the SKS algorithm. This leads to the conclusion that it

is difficult to identify a genuinely representative network geometry. A finer model grid and a higher number of model simulations may lead to a more distinct result.

4. Discussion

The presented Karst Probability Map shows the highest degree of karstification close to the Yarkon spring, in the central part of the model domain, and along the confinement line. This is consistent with the depicted karst abundance map of Laskow et al. (2011) and the discretization of Abusaada and Sauter (2013). The area adjacent to the karst spring and the confinement line, characterized by a steep hydraulic gradient vertical to that line (Dafny et al., 2010), can be interpreted as a region of decreased flow cross-sectional area, vertical to the hydraulic gradient, and thus increased flow velocities resulting in increased carbonate dissolution rates and intensified karstification.

The general distribution of karstification in the model domain indicates that the different phases of karst development strongly influence the geometry and connectivity of the resulting conduit network. This is shown in the map by widespread karstification in the area surrounding the paleo-canyons, also indicated as a "Medium abundance of karst systems" by Laskow et al. (2011). Process models of karst aquifer genesis (e.g., Liedl et al., 2003) show that the largest conduit diameters develop not at the inlet of a conduit where the highest degree of undersaturation concerning calcite is observed, but at the outlet of the karst system, where flow convergence and therefore highest flow velocities occur. The theoretical karst development model results are supported by the high to medium transmissivities measured in boreholes near the canyons (Dafny et al., 2010; Laskow et al., 2011). Recent studies by Paldor et al. (2019, 2020) have begun to investigate by numerical simulations the possible offshore discharge of fresh and brackish water from the WMA through submarine canyons that still occur today.

Reconstruction of the sea-level development along the Israeli coastline from sediment records for example, as done by Rohling et al. (2014) for the whole Eastern Mediterranean Sea, allows for further identification of stages of increased hydraulic gradients and therefore phases of karstification for the WMA. So far, sea levels were reconstructed in the studied region only for individual geological periods: by Flexer et al. (1986) for the Cretaceous, the time of the deposition of the WMA, partly by Druckman et al. (1995) for the Oligocene when the paleo-canyons developed, and by Sivan et al. (2001) for the Holocene, the most recent geological epoch.

Karstification within the recharge area and around the northern Taninim spring cannot be replicated by the Probability Map as clearly as in the surroundings of the Yarkon spring. Further field investigations of individual sinks or dolines in the recharge area may assist to improve the SKS simulations (inputs can be easily adjusted) and help to obtain a better picture of the karstification in these areas. Also identified inlet and outlet locations from large-scale tracer experiments in the study area are helpful (if accessible) to test resulting conduit network geometries, as was done in previous studies where the SKS algorithm has been applied (Borghi et al., 2016; Fandel et al., 2021; Sivelle et al., 2020).

An optimization of all parameters in SKS for the simulation of the conduit network geometry requires major computational effort for example, Fandel et al. (2021). For that reason, we limited the number of model runs to 500 in our sensitivity analysis. Its goal was to investigate the effect of the variability in the location of the start and end points and the effect of the parametrization of the fracture network on the modeled conduit network geometry. Statistically generated inlet and outlet point locations can all justifiably be considered equiprobable within the known boundaries. Locations of in- and outlet points can change because our model accounts for different karstification phases during the past. We found that our results were robust and not significantly affected by the exact position of inlet and outlet points or by the exact fracture parameters. Investigating the effect of the parametrization of the geometric fracture properties on the modeled conduit network geometry during additionally model realizations by reasonably adjusting the variability of values in the built-in Fractur Generator of the SKS algorithm (Table 1) has shown to be of limited impact on the results when using an ensemble modeling approach. These results are in agreement with the observations of Borghi et al. (2012) who discussed the sensitivity of input parameter variation on individual conduits. The MDS analysis uses a pixel-by-pixel-based comparison to define the distances between the conduit networks. Pixel-based distances are not ideal to compare graph-like models. However, within the scope of this study, the method still provides reasonable result, similar to what was shown in Somogyvári et al. (2017). Yet, in future works, we recommend using simulation-based distances, comparing for example, the connectivity properties of the networks.

For the SKS model results to be employed for groundwater model parametrization, suitable conceptual as well as mathematical techniques will have to be employed to generate volume averaged representative continuum hydraulic conductivities. In this study, the SKS is used in a forward modeling approach based on independently determined input parameters such as inlet location, discharge base levels, and the geometry and type of structural features that is, the probability map is not calibrated against measured hydraulic parameters.

The following generalization can be drawn from applying the SKS algorithm to the WMA to provide a useful basis for the parametrization of groundwater models and to acknowledge the uncertainty in modeling these karst structures: (a) the SKS algorithm is a useful tool to test different hypothesis of karst development. Past phases of karst development can strongly influence the present-day flow regime in karst aquifers. Accounting for different karstification phases can improve the accuracy of groundwater models of these aquifers. (b) The SKS algorithm can be applied on a large scale. So far, the SKS algorithm has been used to reconstruct individual karst conduit networks. In this study, we show that (c) the presented methodology can represent uncertainties in conduit network geometry predictions by exploring the stochastic nature of the SKS algorithm. The simplifying approximations made by the SKS algorithm for conduit simulation (Borghi et al., 2012) can (d) considerably reduce computational effort and allow for statistical analysis. After converting the discrete conduit network and the coupled matrix into a volume-averaged continuum hydraulic parameter, it is then possible to implement the representative conduit networks into numerical groundwater models. (e) Finally, the point cloud of the MDS helps to identify representative groups of conduit network realizations.

5. Conclusions

This study presents a stochastic modeling approach to predict on a regional scale the spatial distribution and its uncertainty of a karst conduit network of a highly managed carbonate aquifer system. It can be concluded that from "soft input information" on the karst system alone, a sound Karst Probability Map can be generated, as comparisons with transmissivity field data and previous studies demonstrate. The conceptual model of the karst aquifer genesis, such as paleo-recharge and discharge locations, has a major impact on the connectivity and thus the hydraulics of the resulting conduit network. The SKS algorithm proves to be a useful tool to test the presented conceptual model of karst conduit evolution of the investigated aquifer system and to account for uncertainties of its conduit network. This is especially relevant for modeling karst aquifer systems on a regional scale, where spatial information about the conduit network is otherwise rarely available. In the next step, the assembled conduit network realizations can be transformed into a 3-D Karst Probability Map. The resulting map or individual representative networks could then be used for the parameterization of the hydraulic parameter field of numerical karst groundwater models, improving the understanding and thereby the management of these complex hydrogeological environments.

Data Availability Statement

All climatic input data (precipitation and temperature), realizations for the five hundred 3D conduit networks (.vtk output files) generated with the SKS algorithm, and the point cloud in Figure 8 are available here: https://doi.org/10.14279/depositonce-16021. A readme file to explain the data and overview and further explanations of the parameters assigned to the Fast-Marching-Algorithm in this study is also stored.

Acknowledgments
This research was funded by the German Federal Ministry of Education and Research (grant: 02WGR1428A). The provision of transmissivity data by Joseph Guttman is gratefully acknowledged. Open Access funding enabled and organized by Projekt DEAL.

References

Abusaada, M., & Sauter, M. (2013). Studying the flow dynamics of a karst aquifer system with an equivalent porous medium model. *Groundwater*, *51*(4), 641. https://doi.org/10.1111/j.1745-6584.2012.01003.x

Anderson, M. P., Woessner, W. W., & Hunt, R. J. (2015). *Applied groundwater modeling* (2nd ed.). Academic Press. https://doi.org/10.1016/C2009-0-21563-7

Bakalowicz, M. (2005). Karst groundwater: A challenge for new resources. *Hydrogeology Journal*, *13*(1), 148–160. https://doi.org/10.1007/s10040-004-0402-9

Bartov, Y., Arkin, Y., Lewy, Z., & Mimiran, Y. (1981). *Regional stratigraphy of Israel: A guide to geological mapping*. Geological Survey of Israel.

Bauer, S., Liedl, R., & Sauter, M. (2003). Modeling of karst aquifer genesis: Influence of exchange flow. *Water Resources Research*, *39*(10), 1–12. https://doi.org/10.1029/2003WR002218

Borghi, A., Renard, P., & Cornaton, F. (2016). Can one identify karst conduit networks geometry and properties from hydraulic and tracer test data? *Advances in Water Resources*, *90*, 99–115. https://doi.org/10.1016/j.advwatres.2016.02.009

Borghi, A., Renard, P., & Jenni, S. (2012). A pseudo-genetic stochastic model to generate karstic networks. *Journal of Hydrology*, *414*(415), 516–529. https://doi.org/10.1016/j.jhydrol.2011.11.032

Caers, J., Park, K., & Scheidt, C. (2010). Modeling uncertainty of complex Earth systems in metric space. In *Handbook of geomathematics* (pp. 865–889). Springer Berlin Heidelberg. https://doi.org/10.1007/978-3-642-01546-5_29

Dafny, E., Burg, A., & Gvirtzman, H. (2010). Effects of karst and geological structure on groundwater flow: The case of Yarqon-Taninim Aquifer, Israel. *Journal of Hydrology*, *389*(3–4), 260–275. https://doi.org/10.1016/j.jhydrol.2010.05.038

Druckman, Y., Buchbinder, B., Martinotti, G. M., Tov, R. S., & Aharon, P. (1995). The buried Afiq canyon (Eastern Mediterranean, Israel): A case study of a tertiary submarine canyon exposed in Late Messinian times. *Marine Geology*, *123*(3–4), 167–185. https://doi.org/10.1016/0025-3227(94)00127-7

Dvory, N. Z., Livshitz, Y., Kuznetsov, M., Adar, E., & Yakirevich, A. (2016). The effect of hydrogeological conditions on variability and dynamic of groundwater recharge in a carbonate aquifer at local scale. *Journal of Hydrology*, *535*, 480–494. https://doi.org/10.1016/j.jhydrol.2016.02.011

Eisenlohr, L., Bouzelboudjen, M., Király, L., & Rossier, Y. (1997). Numerical vs. statistical modeling of natural response of a karst hydrogeological system. *Journal of Hydrology*, *202*(1–4), 244–262. https://doi.org/10.1016/S0022-1694(97)00069-3

Eyal, Y., Gross, M. R., Engelder, T., & Becker, A. (2001). Joint development during fluctuation of the regional stress field in Southern Israel. *Journal of Structural Geology*, *23*(2–3), 279–296. https://doi.org/10.1016/S0191-8141(00)00096-1

Fandel, C., Ferré, T., Chen, Z., Renard, P., & Goldscheider, N. (2021). A model ensemble generator to explore structural uncertainty in karst systems with unmapped conduits. *Hydrogeology Journal*, *29*(1), 229–248. https://doi.org/10.1007/s10040-020-02227-6

Fleischer, L., & Gafsou, R. (2003). *Top Judea Group digital structural map of Israel, Scale 1:200,000 (2 sheets)*. Geophysical Institute of Israel.

Flexer, A., Rosenfeld, A., Lipson-Benitah, S., & Honigstein, A. (1986). Relative sea level changes during the Cretaceous in Israel. *AAPG Bulletin*, *70*(11), 1685–1699.

Ford, D., & Williams, P. (2007). Karst hydrogeology and geomorphology. In *Karst hydrogeology and geomorphology*. John Wiley & Sons Ltd. https://doi.org/10.1002/9781118684986

Frantz, Y., Collon, P., Renard, P., & Viseur, S. (2021). Analysis and stochastic simulation of geometrical properties of conduits in karstic networks. *Geomorphology*, *377*, 107480. https://doi.org/10.1016/j.geomorph.2020.107480

Frumkin, A., & Fischhendler, I. (2005). Morphometry and distribution of isolated caves as a guide for phreatic and confined paleohydrological conditions. *Geomorphology*, *67*(3–4), 457–471. https://doi.org/10.1016/j.geomorph.2004.11.009

Garcia-Castellanos, D., & Villaseñor, A. (2011). Messinian Salinity Crisis regulated by competing tectonics and erosion at the Gibraltar arc. *Nature*, *480*(7377), 359–363. https://doi.org/10.1038/nature10651

Goldscheider, N., Chen, Z., Auler, A. S., Bakalowicz, M., Broda, S., Drew, D., et al. (2020). Global distribution of carbonate rocks and karst water resources. *Hydrogeology Journal*, *28*(5), 1661–1677. https://doi.org/10.1007/s10040-020-02139-5

Guttman, J. (2021). The Yarkon-Taninim basin—An example of a major carbonate aquifers in Israel. In *The many facets of Israel's hydrogeology* (pp. 7–25). Springer. https://doi.org/10.1007/978-3-030-51148-7_2

Hill, M. C., Banta, E. R., Harbaugh, A. W., & Anderman, E. R. (2000). *MODFLOW-2000, the U.S. Geological Survey modular ground-water model—User guide to the observation, sensitivity, and parameter-estimation processes and three post-processing programs*. U.S. Geological Survey. https://doi.org/10.3133/ofr00184

Jaquet, O., Siegel, P., Klubertanz, G., & Benabderrhamane, H. (2004). Stochastic discrete model of karstic networks. *Advances in Water Resources*, *27*(7), 751–760. https://doi.org/10.1016/j.advwatres.2004.03.007

Jiménez, S., Mariethoz, G., Brauchler, R., & Bayer, P. (2016). Smart pilot points using reversible-jump Markov-chain Monte Carlo. *Water Resources Research*, *52*(5), 3966–3983. https://doi.org/10.1002/2015WR017922

Kaufmann, G., & Braun, J. (2000). Karst Aquifer evolution in fractured, porous rocks. *Water Resources Research*, *36*(6), 1381–1391. https://doi.org/10.1029/1999WR900356

Kaufmann, G., Romanov, D., & Dreybrodt, W. (2019). Modeling the evolution of karst aquifers. In *Encyclopedia of caves* (3rd ed., pp. 717–724). Academic Press. https://doi.org/10.1016/B978-0-12-814124-3.00086-8

Kovács, A., & Sauter, M. (2007). Modeling karst hydrodynamics.

Krijgsman, W., Hilgen, F. J., Raffi, I., Sierro, F. J., & Wilson, D. S. (1999). Chronology, causes, and progression of the Messinian Salinity Crisis. *Nature*, *400*(6745), 652–655. https://doi.org/10.1038/23231

Laskow, M., Gendler, M., Goldberg, I., Gvirtzman, H., & Frumkin, A. (2011). Deep confined karst detection, analysis, and paleo-hydrology reconstruction at a basin-wide scale using new geophysical interpretation of borehole logs. *Journal of Hydrology*, *406*(3–4), 158–169. https://doi.org/10.1016/j.jhydrol.2011.06.011

Liedl, R., Sauter, M., Hückinghaus, D., Clemens, T., & Teutsch, G. (2003). Simulation of the development of karst aquifers using a coupled continuum pipe flow model. *Water Resources Research*, *39*(3). https://doi.org/10.1029/2001WR001206

Paldor, A., Katz, O., Aharonov, E., Weinstein, Y., Roditi-Elasar, M., Lazar, A., & Lazar, B. (2020). Deep submarine groundwater discharge—Evidence from Achziv Submarine Canyon at the exposure of the Judea Group Confined Aquifer, Eastern Mediterranean. *Journal of Geophysical Research: Oceans*, *125*(1). https://doi.org/10.1029/2019JC015435

Paldor, A., Shalev, E., Katz, O., & Aharonov, E. (2019). Dynamics of saltwater intrusion and submarine groundwater discharge in confined coastal aquifers: A case study in northern Israel. *Hydrogeology Journal*, *27*(5), 1611–1625. https://doi.org/10.1007/s10040-019-01958-5

Pardo-Igúzquiza, E., Dowd, P. A., Xu, C., & Durán-Valsero, J. J. (2012). Stochastic simulation of karst conduit networks. *Advances in Water Resources*, *35*, 141–150. https://doi.org/10.1016/j.advwatres.2011.09.014

Parise, M., Gabrovsek, F., Kaufmann, G., & Ravbar, N. (2018). Recent advances in karst research: From theory to fieldwork and applications. *Geological Society Special Publication*, *466*(1), 1–24. https://doi.org/10.1144/SP466.26

Rohling, E. J., Foster, G. L., Grant, K. M., Marino, G., Roberts, A. P., Tamisiea, M. E., & Williams, F. (2014). Sea-level and deep-sea-temperature variability over the past 5.3 Myr. *Nature*, *508*(7497), 477–482. https://doi.org/10.1038/nature13230

Roveri, M., Flecker, R., Krijgsman, W., Lofi, J., Lugli, S., Manzi, V., et al. (2014). The Messinian Salinity Crisis: Past and future of a great challenge for marine sciences. *Marine Geology*, *352*, 25–58. https://doi.org/10.1016/j.margeo.2014.02.002

Sagy, Y., Gvirtzman, Z., & Reshef, M. (2018). 80 m.y. of folding migration: New perspective on the Syrian arc from Levant Basin analysis. *Geology*, *46*(2), 175–178. https://doi.org/10.1130/G39654.1

Sethian, J. A. (1996). A fast marching level set method for monotonically advancing fronts. *Proceedings of the National Academy of Sciences of the United States of America*, *93*(4), 1591–1595. https://doi.org/10.1073/pnas.93.4.1591

Sethian, J. A. (1999). *Level set methods and fast marching methods: Evolving interfaces in computational geometry, fluid mechanics, computer vision, and materials science* (2nd ed.). Cambridge University Press.

Sethian, J. A. (2001). Evolution, implementation, and application of level set and fast marching methods for advancing fronts. *Journal of Computational Physics*, *169*(2), 503–555. https://doi.org/10.1006/jcph.2000.6657

Sheffer, N. A., Cohen, M., Morin, E., Grodek, T., Gimburg, A., Magal, E., et al. (2011). Integrated cave drip monitoring for epikarst recharge estimation in a dry Mediterranean area, Sif Cave, Israel. *Hydrological Processes*, *25*(18), 2837–2845. https://doi.org/10.1002/hyp.8046

Sivan, D., Wdowinski, S., Lambeck, K., Galili, E., & Raban, A. (2001). Holocene sea-level changes along the Mediterranean coast of Israel, based on archaeological observations and numerical model. *Paleogeography, Paleoclimatology, Paleoecology*, *167*(1–2), 101–117. https://doi.org/10.1016/s0031-0182(00)00234-0

Sivelle, V., Renard, P., & Labat, D. (2020). Coupling SKS and SWMM to solve the inverse problem based on artificial tracer tests in karstic aquifers. *Water*, *12*(4), 1139. https://doi.org/10.3390/w12041139

Somogyvári, M., Jalali, M., Jimenez Parras, S., & Bayer, P. (2017). Synthetic fracture network characterization with transdimensional inversion. *Water Resources Research*, *53*(6), 5104–5123. https://doi.org/10.1002/2016WR020293

Stevanović, Z. (2019). Karst waters in potable water supply: A global scale overview. *Environmental Earth Sciences*, *78*(23), 662. https://doi.org/10.1007/s12665-019-8670-9

UN-ESCWA, & BGR. (2013). Chapter 19—Western aquifer basin. In *Inventory of shared water resources in western Asia* (pp. 461–484). United Nations Publication.

Vuilleumier, C., Borghi, A., Renard, P., Ottowitz, D., Schiller, A., Supper, R., & Cornaton, F. (2013). A method for the stochastic modeling of karstic systems accounting for geophysical data: An example of application in the region of Tulum, Yucatan Peninsula (Mexico). *Hydrogeology Journal*, *21*(3), 529–544. https://doi.org/10.1007/s10040-012-0944-1

Weinberger, G., Rosenthal, E., Ben-Zvi, A., & Zeitoun, D. G. (1994). The Yarkon-Taninim groundwater basin, Israel hydrogeology: Case study and critical review. *Journal of Hydrology*, *161*(1–4), 227–255. https://doi.org/10.1016/0022-1694(94)90130-9

Zanini, A., Feo, A., Petrella, E., & Celico, F. (2021). Groundwater modeling in karst areas. *Water*, *13*(6), 10–12. https://doi.org/10.3390/w13060854